Self-averaging, distribution of pseudocritical temperatures, and finite size scaling in critical disordered systems

Shai Wiseman and Eytan Domany
Department of Physics of Complex Systems, Weizmann Institute of Science, Rehovot 76100, Israel
(Received 9 February 1998)

We evaluate by Monte Carlo simulations various singular thermodynamic quantities X for ensembles of quenched random Ising and Ashkin-Teller models. The measurements are taken at T_c and we study how the distributions $P(X)$ (and, in particular, their relative squared width, R_X) over the ensemble depend on the system size l. The Ashkin-Teller model was studied in the regime where bond randomness is irrelevant and we found weak self-averaging; $R_X \sim l^{\alpha/\nu} \to 0$, where $\alpha < 0$ and ν are the exponents (of the pure model fixed point) governing the transition. For the site-dilute Ising model on a cubic lattice, known to be governed by a random fixed point, we find that R_X tends to a constant, as predicted by Aharony and Harris. We tested whether this constant is universal. However, this constant is different for canonical and grand canonical disorder. We identify the pseudocritical temperature of each sample i, $T_c(i,l)$, as the temperature at which the susceptibility reaches its maximal value $\chi^{\max}$. The distribution of these sample dependent $T_c(i,l)$ was investigated; we found that its variance scales as $[\delta T_c(l)]^2 \sim l^{-2/\nu}$. Our previously proposed finite size scaling ansatz for disordered systems was tested and found to hold. We did observe deviations from a single function, which imply that sample dependent scaling functions are needed. These deviations are, however, relatively small and hence to obtain a fixed statistical error it may be more computationally efficient to measure $\chi^{\max}$ than the commonly used $\chi(T_c^{\infty})$. [S1063-651X(98)10309-4]

PACS number(s): 05.50.+q, 75.10.Nr, 75.40.Mg, 75.50.Lk

I. INTRODUCTION

The critical behavior of randomly disordered systems has been extensively studied [1] experimentally, analytically [2], and numerically [3] for quite some time now. The Harris criterion [4,1,5] states that the critical behavior of the pure system (p) is unaltered by disorder if $\alpha_p < 0$; if $\alpha_p > 0$, even a weakly disordered system will not belong to the same universality class as the pure one. In renormalization group (RG) terminology, the system crosses over from its pure fixed point to a random one. If $\alpha_p = 0$ the situation is marginal.

None of the currently used Monte Carlo (MC) methods can check directly whether a certain model is governed by a pure or disordered fixed point. Numerical studies of disordered systems near their critical points use finite samples; each sample i is a particular random realization of the quenched disorder. A measurement of any *density* of an extensive thermodynamic property X (e.g., X can be the energy E, magnetization M, specific heat C, or susceptibility χ) yields a different value for the exact thermal average X_i of every sample i. In an ensemble of disordered samples of linear size l the values of X_i are distributed with a probability distribution $P_l(X)$. Most MC studies determine only the ensemble average $[X]_l$. In this study we show that by studying $P_l(X)$, MC can yield direct evidence about the nature of the governing fixed point. This can be done by studying the question of *self-averaging*, namely, the behavior of the width of $P_l(X)$ as the system size l increases. We characterize $P(X)$ by its average $[X]$ and relative variance R_X,

$$R_X = V_X/[X]^2, \quad V_X = [X^2] - [X]^2. \tag{1}$$

Suppose that X is a singular density of an extensive thermodynamic property, such as M, χ, or the singular part of E or C. The system is said to exhibit *self-averaging* [6] if

$$R_X(l) \to 0 \quad \text{as} \quad l \to \infty. \tag{2}$$

If R_X tends to a constant different from zero, the system exhibits a *lack of self-averaging*. In a self-averaging system a single very large sample suffices to represent the ensemble; without self-averaging, a measurement performed on a single sample, no matter how large, does not give a meaningful result and must be repeated on many samples. In a MC study of a self-averaging disordered system the number of samples needed to obtain $[X]$ to a given relative accuracy decreases with increasing l. On the other hand, in a non-self-averaging system the number of samples that must be simulated is independent of l and the total amount of work rises very strongly with l.

Off criticality, where l is much larger than the correlation length ξ, as first argued by Brout [7], we may divide the sample i into n large subsamples (much larger than ξ). Neglecting the coupling between subsystems, the measured value X_i is equal to the average of this quantity over the (independent) subsamples. According to the central limit theorem, X_i is distributed normally around its mean $[X_i]$ with variance $V_X \propto 1/n \sim l^{-d}$. In such a case, where $R_X \sim l^{-d}$, X is called *strongly self-averaging* [8].

Close to criticality, where $\xi \sim l$, the Brout argument does not hold, since the subsamples are not independent. Thus at criticality there is no reason to expect that $R_X \sim l^{-d}$. To test this possibility we investigated [9] a family of random-bond Ashkin-Teller models with $\alpha_p > 0$, i.e., relevant randomness, and discovered lack of self-averaging for various quantities measured at T_c^{∞} (another report on lack of self-averaging can be found in [17]). This finding has far reaching conse-

quences; in particular, the standard way of measuring some X at T_c^∞ and analyzing its size dependence using standard finite size scaling breaks down, since the sample dependence of X needs to be taken into account. As the system size increases, one moves also to a different realization of the randomness; lack of self-averaging implies that the only quantity whose dependence on l provides meaningful information is the distribution $P_l(X)$. Thus the need for a new finite size scaling theory, suitable for these circumstances, arose. We proposed such a theory, postulating, following Harris, that one can characterize every sample i of size l by the sample dependent reduced temperature

$$\dot{t}_i = \frac{T - T_c(i,l)}{T_c} \tag{3}$$

where $T_c(i,l)$ is a sample dependent pseudocritical temperature, which fluctuate around its ensemble average $T_c(l)$ with width $\delta T_c(l)$. A sample dependent finite size scaling form

$$X_i(T,l) = l^\rho \tilde{Q}_i(\dot{t}_i l^{y_t}) \tag{4}$$

was introduced; the exponent ρ characterizes the behavior of $[X]$ at T_c; e.g., for $X=\chi$, $\rho=\gamma/\nu$. Next we assumed that the pseudocritical temperatures are distributed with a width $\delta T_c(l)$ that scales as

$$[\delta T_c(l)]^2 \sim l^{-d}. \tag{5}$$

Combining this with our scaling ansatz (4) we predicted that if the specific heat exponent of the *disordered model* $\alpha<0$ then, at criticality,

$$R_X \sim l^{\alpha/\nu}. \tag{6}$$

Thus, if $\alpha/\nu=0$, X is non-self-averaging, but if $-d<\alpha/\nu<0$, X is called *weakly self averaging* [8]. Note that according to [10] $\alpha/\nu \leqslant 0$ in any disordered system, though claims to the contrary exist (e.g., [11] and [12]).

In the present manuscript we extend our work in several directions that were not considered previously and, in particular, test our prediction against a renormalization group study of the problem, performed [13] by Aharony and Harris (AH). These authors found that when the system is governed by a random fixed point, $P(X)$ approaches a universal, l independent shape, and $R_X \to$ const as $l \to \infty$, which implies lack of self-averaging. When randomness is irrelevant, their prediction for R,

$$R_X \sim l^{(\alpha/\nu)_p} \tag{7}$$

coincides with Eq. (6). The new questions we ask are the following:

(1) We test our prediction (6) to cases with *irrelevant randomness*.

(2) We study the *three-dimensional* site-random Ising model. Here randomness is relevant, $\alpha_p \approx 0.11$ [18], and the random specific heat exponent is known to be *negative* [19,20]. Hence the AH prediction $R \to$ const is in clear contradiction of ours, Eq. (6).

(3) As AH point out, this disagreement between the RG result and our scaling ansatz can be reconciled if we assume that in disordered systems governed by a random fixed point, Eq. (5) is substituted by

$$[\delta T_c(l)]^2 \sim l^{-2/\nu}. \tag{8}$$

The manner in which $\delta T_c(l)$ scales for relevant randomness is an important issue whose resolution will bear on our understanding of a variety of random systems [12]. A direct study of how $\delta T_c(l)$ scales is carried out; we calculated the pseudocritical temperature (defined as the maximum of χ) for an ensemble of site-diluted 3D Ising samples, using the histogram reweighting method [21–25].

(4) By working at different dilutions and different ensembles of random systems we test the AH prediction regarding the *universality* of R.

(5) We test the validity of the finite size scaling ansatz Eq. (4), in particular, the extent to which the dependence on the realization can be absorbed entirely in the sample-dependent pseudocritical temperature.

This work is organized as follows. In the first part of Sec. II we define the random bond Ashkin-Teller model, which was simulated and summarize its critical behavior as found by the finite size scaling results. In the second part of Sec. II we give our results concerning self-averaging at criticality. The results indicate clearly that R_X is weakly self-averaging and are in good agreement with Eq. (7). In Sec. III we summarize some relevant properties of the site-dilute Ising model on a cubic lattice and give some details of the simulation. Finite size scaling results for some observables at criticality are given as well. In Sec. IV we analyze and discuss our results concerning self-averaging at T_C^∞. These results seem to indicate the correctness of the AH scenario, whereby R_X is non-self-averaging. In Sec. V we study the distributions of the pseudocritical temperatures of the site-dilute Ising model. The scaling of $[\delta T_c(l)]^2$ does not agree with Eq. (5) but seems to agree with Eq. (8), giving additional evidence for the validity of the AH scenario. In Sec. V we also analyze the distributions of the maximal susceptibilities $\chi(T_c(i,l))$, and investigate the extent to which the scaling form (4) holds. The work is summarized in Sec. VI. A condensed account of this work can be found in [47].

II. WEAK SELF-AVERAGING IN AN ASHKIN-TELLER MODEL WITH IRRELEVANT DISORDER

A. Definition of the model

The model we study is the random-bond Ashkin-Teller model on a square lattice. On every site of the lattice two Ising spin variables, σ_i and τ_i, are placed. Denoting by $\langle ij \rangle$ a pair of nearest neighbor sites, the Hamiltonian is given by

$$\mathcal{H} = -\sum_{\langle ij \rangle} [K_{i,j}(\sigma_i \sigma_j + \tau_i \tau_j) + \Lambda_{i,j} \sigma_i \tau_i \sigma_j \tau_j]. \tag{9}$$

$K_{i,j}$ and $\Lambda_{i,j}$ are chosen according to

TABLE I. Estimates for critical exponent ratios of the Ashkin-Teller models from finite size scaling at T_c^{∞} obtained with linear fits to $\ln l$ according to Eqs. (15)–(17).

	α/ν	β/ν	γ/ν	$\beta^{(p)}/\nu$	$\gamma^{(p)}/\nu$	Fitting interval
Random bond	−0.536(32)	0.1252(4)	1.7502(5)	0.322(1)	1.3566(15)	$24 \leqslant l \leqslant 256$
Anisotropic	−0.745(4)	0.1262(2)	1.7488(1)	0.3312(5)	1.339(1)	$16 \leqslant l \leqslant 256$

$$(K_{i,j},\Lambda_{i,j}) = \begin{cases} (K^1,\Lambda^1) & \text{with probability } \frac{1}{2} \\ (K^2,\Lambda^2) & \text{with probability } \frac{1}{2}. \end{cases} \tag{10}$$

The pure model [26] [$(K^1,\Lambda^1)=(K^2,\Lambda^2)\equiv(K,\Lambda)$] flows under RG onto a line of fixed points along which exponents vary continuously. In particular, $\phi=(\alpha/\nu)$, which is analytically known [27,28], varies, along the part of the critical line with $\Lambda \geqslant 0$, and interpolates between the Ising ($\Lambda=0$) and four state Potts ($\Lambda=K$) models ($1 \geqslant \phi \geqslant 0$), so that randomness is relevant. Indeed the critical behavior of the disordered model [15,14,2,16,17] was found to be different from that of the pure one and lack of self-averaging was found [9]. Along the other part of this line ($\Lambda<0$) $\phi=\alpha/\nu$ is negative, so that randomness is irrelevant; a model with finite disorder will flow under RG [2,15] onto a pure model with $\phi=\alpha/\nu<0$, leading to weak self-averaging at criticality.

Part of the critical manifold of the random-bond Ashkin Teller model can be found exactly through duality. In parts of the coupling space where only two phases exist the self-dual manifold

$$(K^2,\Lambda^2)=(\widetilde{K^1},\widetilde{\Lambda^1}) \tag{11}$$

is critical. Here $(\widetilde{K^1},\widetilde{\Lambda^1})$ are the dual couplings of (K^1,Λ^1) [16]. We chose to study a model with the ratio

$$\frac{K^2}{K^1}=\frac{1}{10}, \tag{12}$$

so that randomness will be pronounced. In addition, a ratio of

$$\frac{\Lambda^1}{K^1}=-f=-\frac{9}{10} \tag{13}$$

was chosen. Since α/ν decreases as f increases and $\alpha/\nu=0$ for $f=0$ (Ising model), we have chosen $f=\frac{9}{10}$ so that α/ν will be a pronounced negative number. Equations (11)–(13) define the couplings of the model simulated, where the temperature T was absorbed into the couplings K_{ij},Λ_{ij}.

An *anisotropic Ashkin-Teller* model is used as a reference pure model [16]; it has the same Hamiltonian (9) but with

$$(K_{i,j},\Lambda_{i,j}) = \begin{cases} (K^1,\Lambda^1) & \text{for bonds } (i,j) \text{ in the horizontal direction} \\ (K^2,\Lambda^2) & \text{for bonds } (i,j) \text{ in the vertical direction .} \end{cases} \tag{14}$$

In our Monte Carlo simulations we used a cluster algorithm [29,30] described in [16]. The number of samples simulated was $n=2000$ for linear lattice sizes $4 \leqslant l \leqslant 64$, $n(128)=1200$ for $l=128$, and $n(256)=436$. For each sample i Monte Carlo estimates of various observables $\overline{X_i}$ and their errors $\delta\overline{X_i}$ were calculated.

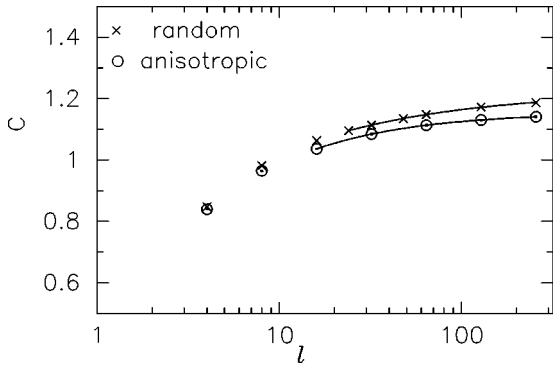

FIG. 1. The specific heat C of the random bond and the anisotropic Ashkin-Teller models as a function of $\log_{10} l$. The solid lines are fits to the form (15).

B. Critical behavior of the model

Here we give the finite size dependences of averages (over all samples) of various observables, defined as in [16], at the critical point T_c^{∞} defined through Eqs. (11)–(13).

In Fig. 1 we plot the specific heat of the random bond and the anisotropic models as a function of $\log_{10} l$. The solid lines are fits to the finite size scaling form

$$C=B_0+B_1 l^{\alpha/\nu}. \tag{15}$$

Using lattice sizes of $16 \leqslant l \leqslant 256$, we find $\alpha/\nu=-0.745(4)$ for the anisotropic model, while using lattice sizes of $24 \leqslant l \leqslant 256$, we find $\alpha/\nu=-0.536(32)$ for the random bond model (note, B_1 is negative). Thus this strongly disordered model apparently flows under RG onto a pure model with different exponents than its anisotropic version but still one that is along the part of the line of fixed points where $(\alpha/\nu)_p<0$.

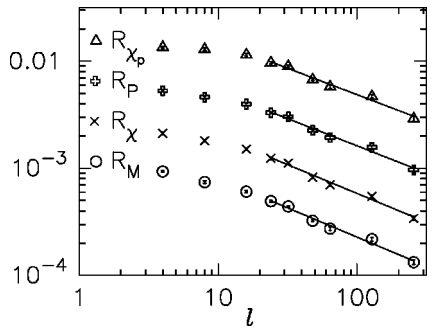

FIG. 2. The relative variance of the susceptibility R_χ, of the magnetization R_m, of the polarization R_P, and of the polarization susceptibility $R_{\chi^{(p)}}$ of the Ashkin-Teller model at T_c^∞ as a function of $\log_{10} l$. The solid lines are linear fits according to Eq. (19).

For both models the magnetization m and susceptibility χ were fitted to the forms

$$m = A_m l^{-\beta/\nu} \quad \chi = A_\chi l^{\gamma/\nu}. \tag{16}$$

Similarly the polarization P (magnetization of the τ spins) and susceptibility of the polarization $\chi^{(p)}$ were fitted to the forms

$$P = A_P l^{-\beta^{(p)}/\nu} \quad \chi^{(p)} = A_{\chi^{(p)}} l^{\gamma^{(p)}/\nu}. \tag{17}$$

The estimates for the exponent ratios obtained are listed in Table I. The values of β/ν and γ/ν are within errors, for the random bond model or very close, for the anisotropic model, to the Ising exponent ratios $\beta/\nu = \frac{1}{8}$ and $\gamma/\nu = \frac{7}{4}$. These exponent ratios are predicted analytically [27,28] to be of this magnitude all along the critical line of the pure Ashkin-Teller model.

C. Calculation of V_X

The variance σ_X^2 of the Monte Carlo estimates $\overline{X_i}$ is the sum of two contributions. The main contribution is due to the variance V_X of the distribution of the true X_i. V_X is the quantity we wish to study. The second contribution is due to the errors of the estimated observables, $\delta\overline{X_i}$. Thus, the unbiased estimator [31] of the variance of the X_i is

$$V_X = \sigma_X^2 - [(\delta\overline{X_i})^2]. \tag{18}$$

$\delta\overline{X_i}$ depends on the length of the MC runs and on the autocorrelation time τ_X of the MC dynamics. To obtain a valid estimate of V_X, $[(\delta\overline{X_i})^2]/V_X$ should be sufficiently small. In the random bond Ashkin-Teller model studied here this requirement was not met for the specific heat C, whereby we could not study R_C. Additional discussion of the practical implications of Eq. (18) can be found in Sec. III of [9]. Next we list results concerning the critical behavior of V_X at T_c^∞.

D. The relative variance R_X

In Fig. 2 we plot R_m, R_χ, R_P, and R_{χ_p} as a function of $\log_{10} l$. The solid lines are linear fits to the form

$$R_X = A_X l^{\rho_X} \tag{19}$$

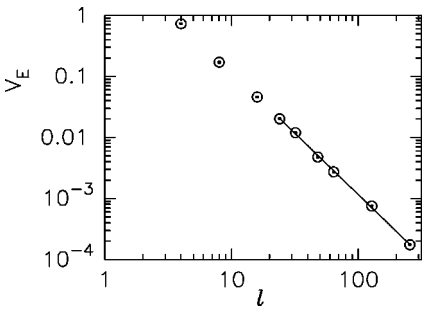

FIG. 3. The variance of the energy V_E of the Ashkin-Teller model at T_c^∞ as a function of $\log_{10} l$. The solid line is a linear fit according to $V_E = A_{vE} l^{x_E}$, yielding $x_E = -2.005(26)$.

for $24 \leqslant l \leqslant 256$. The estimates obtained for ρ_X are $\rho_\chi = -0.537(32)$, $\rho_m = -0.546(38)$, $\rho_{\chi^{(p)}} = -0.493(37)$, and $\rho_P = -0.509(41)$. Clearly all observables, $m, \chi, P, \chi^{(p)}$ are weakly self-averaging. Furthermore ρ_χ and ρ_m are in very good agreement with the value of $\alpha/\nu = -0.536(32)$, while ρ_{χ_p} and ρ_P are also within errors of α/ν. Thus the results for the scaling of the relative variance of these four observables are in good agreement with the predictions of AH and with (6).

For the energy one cannot separate the singular and the analytic parts. In addition, the singular part decays as l^ρ, with $\rho = (\alpha - 1)/\nu$. Using our estimate of $\alpha/\nu = -0.536(32)$ and the hyperscaling relation $\alpha/\nu = 2/\nu - d$, we find $\rho = -1.268(48)$. Thus the variance of the singular part of the energy is expected according to Eq. (6) to scale as $l^{-3.072}$. Therefore one would expect V_E to be dominated by the fluctuations of the analytic part of E decaying as l^{-d}. In Fig. 3 the variance of the energy V_E as a function of $\log_{10} l$ is plotted. Straightforward linear fits to the form $V_E = A_{vE} l^{x_E}$ in the lattice size range $24 \leqslant l \leqslant 256$ yielded $x_E = -2.005(26)$ in good agreement with our expectation $x_E = -d$.

To conclude this part of the study, we found weak self-averaging at criticality for a disordered model governed by a pure fixed point with $(\alpha/\nu)_p < 0$. We also found good agreement with the scaling prediction (7).

III. THE SITE-DILUTE ISING MODEL ON A CUBIC LATTICE

In a site-dilute Ising model (see, e.g., [3] and references therein) on every site of a $l \times l \times l$ cubic lattice either an Ising magnetic spin $S_i = \pm 1$ is placed if $K_i = 1$ or a vacancy is placed if $K_i = 0$. The K_i are randomly drawn according to one of the prescriptions given below. The system is governed by the Hamiltonian

$$\mathcal{H} = -J \sum_{\langle i,j \rangle} K_i S_i K_j S_j, \tag{20}$$

where $\langle i,j \rangle$ stands for a pair of nearest neighbors. RG calculations found a dilution independent random fixed point with universal critical exponents. For example, a recent calculation [20] obtained $\gamma = 1.313$, $\beta = 0.342$ $\nu = 0.666$, and $\alpha = 0.002$. Early MC studies found global effective critical exponents that were found to depend on dilution. This was later interpreted as due to crossover effects. For example, in a

TABLE II. Number of site-dilute samples simulated for each model and lattice size l. The last column lists the infinite lattice critical temperature, as estimated by Heuer [32], at which the simulations were performed. For $c=0.6$, $l=90$ the pseudocritical temperature was not estimated.

	$l=10$	$l=20$	$l=40$	$l=60$	$l=80$	$l=90$	T_c^∞
$c=0.6$	8000	26000	2000	800		1000	2.4220(6)
$p=0.6$	72000	47000	8000	950	800		2.4220(6)
	$l=4$	$l=8$	$l=16$	$l=32$	$l=64$		
$p=0.8$	10000	4000	32000	4000	1479		3.4992(5)

most extensive MC study, Heuer [32] found from finite size scaling in the lattice size range $20\leqslant l\leqslant 60$ values ranging from $(\alpha/\nu)(p=0.95)=0.12(6)$ with 5% vacancies, to $(\alpha/\nu)(p=0.8)=-0.04(6)$ and $(\alpha/\nu)(p=0.6)=-0.22(6)$. However, he argued by analyzing a suitable scaling function that all models with different amounts of dilution are exhibiting a crossover to the fixed point predicted by RG. His results show that, of the amounts of dilution he studied, the $p=0.8$ model reached the universal behavior at the smallest lattice sizes. Later Janssen, Oerding, and Sengespeick [20] showed in their RG calculations that the effective exponent values obtained by Heuer can be related to regions in the space of coupling coefficients away from the fixed point.

A. Details of the simulations

Three site-dilute Ising models were examined, including two types of disorder. In one model disorder was realized in a canonical manner; namely, the number of magnetic sites in each site-diluted sample was fixed at a fraction $c=0.6$ of the number of sites in the lattice. Thus fluctuations among samples occur only in the locations of the magnetic sites but not in their number. In two other models disorder was realized in a grand-canonical manner; namely, each sample was created by assigning to each site of the lattice a magnetic spin (vacancy) with probability p $(1-p)$. In one model we used $p=0.6$ and in the second one $p=0.8$. In this case fluctuations among samples include fluctuations in the number of magnetic sites. These fluctuations tend to zero as $l\to\infty$, but for finite l they are significant. For this reason we found it of interest, in this study of fluctuations among samples, to compare the two ensembles. We are unaware of any previous findings attesting to differences in the asymptotic critical behavior between the two ensembles. Because of the (spatially) uncorrelated nature of the disorder in the grand canonical ensemble it is favored for its relative simplicity by theoretical studies (see [20] for references) and by numerical studies [33–37] aiming to test them. On the other hand, in studying by Monte Carlo *average* thermodynamic observables, errors can be reduced by using canonical disorder, as was done in [32]. We note that if one wishes to study by Monte Carlo simulation the *fluctuations* in the thermodynamic observables due to disorder, the use of grand canonical disorder is advantageous.

In the Monte Carlo simulations we used the Wolff [30] single cluster algorithm [29] for the Ising model because of its efficiency [38]. Skewed periodic boundary conditions [8] were used in order to speed up the simulations. For each model and lattice size n site-dilute samples were simulated. Table II summarizes the number of samples n used for each lattice size for the three models. Simulations were performed at the estimated infinite lattice critical temperatures T_c^∞, given in Table II, due to Heuer [32], and taking $J=1$.

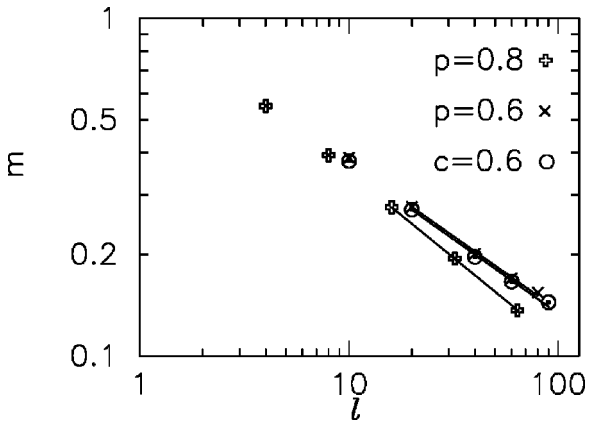

FIG. 4. The magnetization m at T_c^∞ as a function of $\log_{10}l$. The solid lines are fits to the form (16), yielding estimates for β/ν that are listed in Table III.

B. Finite size scaling at T_c^∞

Here we give the finite size dependence of averages (over all samples) of some observables at the critical point $[\overline{X}_i(T_c^\infty)]$.

1. Magnetization m and susceptibility χ_c

Using the abbreviation

$$M=\sum_i K_i S_i, \tag{21}$$

the magnetization density m is defined as

$$m=\frac{[\langle|M|\rangle]}{Np}, \tag{22}$$

where $N=l^3$ and the fraction of magnetic sites was either $p=0.8$ or $p=0.6$. The susceptibility at T_c^∞ was defined as [8]

$$\chi_c=\frac{[\langle M^2\rangle]}{NpT}. \tag{23}$$

The magnetization density m and susceptibility χ_c were fitted to the finite size scaling forms (16).

The estimates that were obtained for the critical exponents ratios β/ν and γ/ν from the fits in Figs. 4 and 5 are listed in Table III together with the estimates of Heuer [32]. Note that exponent ratios and critical temperatures quoted from [32] for $p=0.8$ were actually obtained with canonical disorder $c=0.8$.

2. $\partial m/\partial t$ and estimation of α/ν

In attempting to estimate the exponent ratio α/ν directly from the finite size scaling of the specific heat C through Eq.

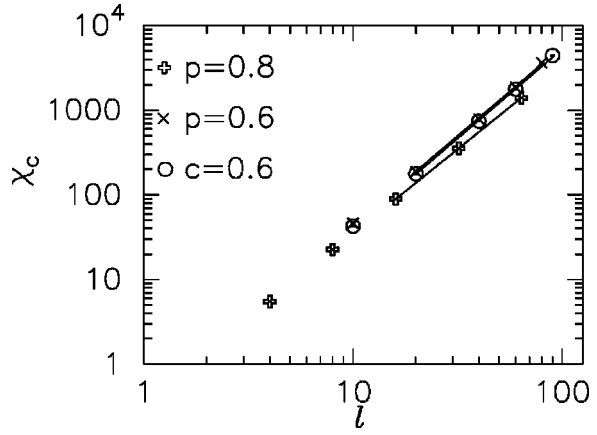

FIG. 5. The susceptibility χ_c as defined in Eq. (23) at T_c^∞ as a function of $\log_{10} l$. The solid lines are fits to the form (16), yielding estimates for γ/ν that are listed in Table III.

(15), we encountered two difficulties. First, we found that the estimates of the specific heat of each sample $\overline{C_i}$ were very sensitive to the length of the simulations. Shorter simulations biased the specific heat to lower values, e.g., for $p=0.6$, $l=40$, the value measured for C using an average simulation length of $n/(2\tau_E+1)\approx 120$ was two standard deviations smaller than the one measured with a four times longer simulation. The systematic underestimation of the response functions due to run lengths that are too short was studied in [39]. Second, the accuracy in estimating α/ν from the specific heat behavior is rather poor. This is due to the fact that α/ν is a small negative number so that the singular behavior of C is difficult to disentangle from other analytic contributions [40].

In order to overcome the difficulty in estimating the exponent ratio α/ν we followed Heuer [40] and measured the derivative of the magnetization with respect to the reduced temperature $t=(T-T_c)/T_c$. It is equal to the magnetization-energy correlation

$$\Gamma=-\frac{\partial m}{\partial t}=-\frac{\partial^2 f}{\partial H\partial t}\approx\frac{-1}{NpT^2}[\langle(|M|-\langle|M|\rangle)(\mathcal{H}-\langle\mathcal{H}\rangle)\rangle], \tag{24}$$

where f is the free energy density. From the scaling behavior of the free energy

$$f(t,h)=b^{-d}f(b^{y_t}t,b^{y_h}h) \tag{25}$$

TABLE III. Estimates for order parameter critical exponent ratios from finite size scaling at T_c^∞. Estimates due to Heuer [32] are listed for comparison. Note that throughout the paper the errors given for our results are only statistical while Heuer's error estimates include the systematic errors that could arise from errors in determining T_c^∞.

	β/ν	β/ν (Heuer)	γ/ν	γ/ν (Heuer)
$c=0.6$	0.438(13)	0.45(2)	2.110(21)	2.09(3)
$p=0.6$	0.437(12)		2.104(20)	
$p=0.8$	0.505(2)	0.51(2)	1.990(4)	1.98(3)

TABLE IV. Estimates for critical exponent ratios from finite size scaling at T_c^∞. Estimates due to Heuer [32] are listed for comparison. The estimate for α/ν is based on the relation $\alpha/\nu=2(\zeta/\nu+\beta/\nu)-d$.

	(ζ/ν)	ζ/ν (Heuer)	(α/ν)	α/ν (Heuer)
$c=0.6$	0.948(6)	0.94(2)	−0.228(28)	−0.22(6)
$p=0.6$	0.958(3)		−0.210(30)	
$p=0.8$	0.962(4)	0.97(2)	−0.066(9)	−0.04(6)

one finds that Γ diverges as $t^{-\zeta}$, where

$$\zeta=\frac{y_t-(d-y_h)}{y_t}=1-\beta. \tag{26}$$

Thus we fit Γ to the finite size scaling form

$$\Gamma=C_0 l^{\zeta/\nu}. \tag{27}$$

The resulting estimates for ζ/ν are given in Table IV. Assuming the hyperscaling relation $\alpha/\nu=2/\nu-d$ and using Eq. (26) the scaling relation $\alpha/\nu=2(\zeta/\nu+\beta/\nu)-d$ is obtained. Using this relation, the results for m and Γ are utilized in Table IV to give estimates for α/ν that are much more accurate than those obtained from analysis of the specific heat results.

IV. LACK OF SELF-AVERAGING AT T_c^∞

In order to obtain the variance V_X and the relative variance R_X the same procedure and considerations as described in Sec. II C were used.

In Fig. 6 we plot the relative variance of the magnetization R_m as a function of lattice size on a double-logarithmic scale. Several interesting features are suggested by this figure. First, note that for $p=0.6$, R_m is decreasing as l increases for the smaller lattice sizes, possibly leveling off for large l. R_m of the $p=0.8$ model first decreases slightly and then seems to tend to a constant. Since it seems plausible that $R_m(p=0.6)\geqslant R_m(p=0.8)$ for any lattice size, these trends seem to imply that for the two grand canonical models R_m tends to the same constant. Assuming that this constant is bound from above by the $p=0.6$ model and from below by the $p=0.8$ model we estimate it as $R_m=0.055(2)$. The implication of this scenario is that R_m of the weakly diluted $p=0.8$ model reaches the universal R_m value of the dilute Ising fixed point at smaller system sizes than the highly diluted $p=0.6$ model. The fluctuations in m_i in the highly

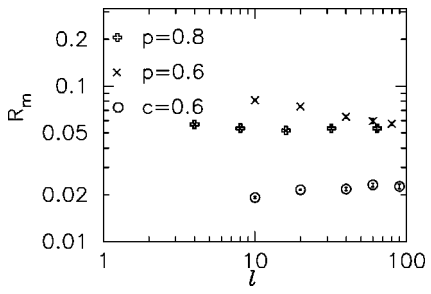

FIG. 6. The relative variance of the magnetization R_m at T_c^∞ as a function of $\log_{10} l$.

TABLE V. Different parameters related to the average pseudocritical inverse temperature $K_{\max}(l)$ and its variance $V_{K_{\max}}$. Second column: estimate of the shift exponent λ according to Eq. (30), where K_c is taken from Heuer [32]. Third and fourth columns: same as first column but with K_c being a free parameter. Fifth column: estimate of y_t based on the finite size scaling of m and Γ. Sixth column: same as fifth according to [32]. Last column: exponent of $V_{K_{\max}}$.

	λ (K_c fixed)	λ	K_c	$y_t=\zeta/\nu+\beta/\nu$	y_t (Heuer)	$\rho_K/2$
$c=0.6$		0.99(19)	0.412 54(13)	1.386(14)	1.39(4)	1.41(4)
$p=0.6$		1.30(10)	0.412 51(5)	1.395(12)		1.421(9)
$p=0.8$	1.446(34)	1.346(2)	0.285 760 9(4)	1.467(5)	1.47(4)	1.44(2)

diluted $p=0.6$ model are larger than those of the dilute Ising fixed point model. This finding is in line with Monte Carlo results [32] and RG calculations [20], according to which the critical exponents of the dilute Ising fixed point are closer, in the lattice size range $20\leqslant l\leqslant 60$, to the observed effective critical exponents of the $p=0.8$ model than to those of the $p=0.6$ model.

A second feature is the striking difference between the two types of disorder, with the canonically disordered $c=0.6$ model exhibiting a much smaller relative variance than that of the two grand canonical disorder models. While R_m of the $c=0.6$ model is initially increasing with system size it appears to level off to a constant value of $R_m(l=90)=0.0227(8)$. Though it is possible that R_m could increase at larger lattice sizes it seems unlikely since the system sizes are already quite large. An indicator to the similarity of the two types of models $p=0.6$ and $c=0.6$ is the relative square root mean of the fluctuations in the number of magnetic sites $\mathcal{N}=\Sigma_{j=1}^{N}K_j$ in the $p=0.6$ systems $\sqrt{[(\mathcal{N}-[\mathcal{N}])^2]/[\mathcal{N}]^2}=\sqrt{(1-p)/Np}$, which for $l=80$ is as small as $\sim\frac{1}{1000}$.

If indeed R_m of the $c=0.6$ model tends to a different constant than that of the models with grand canonical disorder, then according to Aharony and Harris' very general RG arguments [13] the two types of models do *not* belong to the same universality class. We are not aware of any additional evidence to this effect otherwise. For example, our critical exponent estimates for the $c=0.6$ and $p=0.6$ are compatible with each other, and our exponents for the $p=0.8$ model are compatible with those of Heuer [32] for a $c=0.8$ model. The critical temperatures for both types of models seem also to agree (see Table V and Refs. [32,35]). This question is currently under investigation. The results [41] suggest that the two types of models do flow to the same fixed point and that the difference in R_m will disappear for very large l.

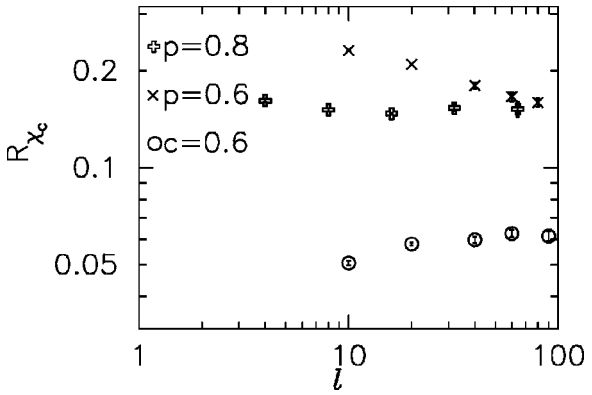

FIG. 7. The relative variance of the susceptibility R_{χ_c} at T_c^∞ as a function of $\log_{10}l$.

The relative variance of the susceptibility R_{χ_c} is plotted in Fig. 7. R_{χ_c} exhibits the same qualitative behavior as that of R_m. R_{χ_c} of the grand canonical disorder models tends to $R_{\chi_c}=0.156(4)$, while R_{χ_c} of the $c=0.6$ model seems to tend to $R_{\chi_c}(l=90)=0.061(2)$. Aharony and Harris [13,42] found that to leading order in $\epsilon=4-d$, $R_M/R_\chi=1/4$. We find that for $p=0.8$ $R_M/R_\chi=0.35(2)$ and for $c=0.6$ $R_M/R_\chi=0.37(1)$. Possibly terms of higher order in ϵ would reconcile this discrepancy. It cannot be attributed to the definition of χ_c. If one defines the susceptibility as in Eq. (28) then at T_c^∞ one finds that R_χ becomes smaller by a factor of $\sim 7-10$. In this case the ratio R_M/R_χ would become even larger. We did not use this definition for the susceptibility at T_c^∞ because of its large single sample errors $\delta\overline{\chi}_i$ (see also [8]).

V. SCALING OF PSEUDOCRITICAL TEMPERATURES

A. Calculating $T_c(i,l)$ with the histogram reweighting method

One of the main purposes of this work was to study the distribution of pseudocritical temperatures $T_c(i,l)$ of the ensemble of site-dilute Ising models. The main aim was to study directly the scaling of $\delta T_c(l)$ with l and test which one of Eqs. (5) or (8) is correct in the case of a system governed by a disordered fixed point. The inverse pseudocritical temperature $K_c(i,l)=1/T_c(i,l)$ of the ith sample was defined as the inverse temperature of the maximum of the susceptibility of that sample, $K_c(i,l)\equiv K_{\max}(i,l)$. Here the definition of the susceptibility was

$$\chi_i=\frac{\langle M^2\rangle-\langle|M|\rangle^2}{NpT}. \tag{28}$$

In order to find $K_{\max}(i,l)$ the following iteration procedure was followed for each sample. A first simulation was performed at the infinite lattice critical temperature (as estimated in [32]) $K_1=K_c^\infty$ (the index i is omitted from here on). In addition to calculating the observables m,χ,Γ, a histogram of the energy and magnetization was generated. Using the single histogram reweighting technique [21–25] (for previous studies of disordered systems utilizing the histogram reweighting technique see [36,43]), this histogram can serve to calculate observables at temperatures close to K_1. By calculating χ at different temperatures a first estimate for the

susceptibility maximum $\chi^1_{\max}$ and the temperature at which it occurs $K^1_{\max}$ was obtained. A second simulation was then performed at a temperature somewhat above this estimate $K_2 = K^1_{\max} - K_{\rm off}$. Previous studies of the histogram reweighting technique have shown that the errors of observables at T, $\delta\overline{X}(T)$, are smaller [25,23] when the temperature at which the histogram was generated $T_{\rm sim}$ is slightly higher, $T_{\rm sim} > T$. For this reason we chose $K_{\rm off}$ to be a small positive number (see more details below).

Using the energy and magnetization histogram generated at K_2 a new estimate for the temperature of the susceptibility maximum, $K^2_{\max}$, was obtained. If the difference between the two estimates was smaller than a predetermined resolution r, $|K^2_{\max} - K^1_{\max}| < r$, the iteration process was stopped. Otherwise the iteration process continued, whereby $K_j = K^{j-1}_{\max} - K_{\rm off}$, until the condition

$$|K^j_{\max} - K^{j-1}_{\max}| < r \tag{29}$$

was met. This iteration process was intended to overcome the problem of systematic errors [23] that occur when the simulation temperature is too far from the true $K_{\max}$. The condition (29) is supposed to ensure that the last two estimates for $K_{\max}$ do not suffer from a systematic error. r was chosen equal to the approximately expected statistical error of $K^j_{\max}$. If the iteration process did not terminate before or with the third estimate $K^3_{\max}$ then the Monte Carlo simulation length at K_4 was doubled and the process was continued. It was again doubled if it reached the seventh iteration and again doubled if it reached the tenth iteration. Nonconvergence of the process after twelve iterations was very rare. In those samples the iteration procedure was restarted manually with $K_1 = K_c^\infty$ but with a larger initial Monte Carlo simulation length. The need to increase the simulation length for some samples occurred because for different samples there were different autocorrelation times (of the Monte Carlo dynamics) and different average cluster sizes, while the simulation length was specified by the *number* of Wolff cluster flips.

In order to estimate the statistical error and reduce it, a simulation with five times as many Monte Carlo steps (compared to the simulation length of the last iteration) was performed again at the last simulation temperature K_j. The Monte Carlo sequence was broken into five, using each segment to create a separate histogram and calculate a separate estimate of $K_{\max}$ and $\chi_{\max}$. Together with the last estimates of $K_{\max}$ and $\chi_{\max}$ of the iteration procedure, all together six estimates of $K_{\max}$ and $\chi_{\max}$ were averaged to give final estimates of $K_{\max,i}$ and $\chi_{\max,i}$. The variance of these six estimates was used to estimate the error for the two quantities, $\delta K_{\max,i}$, and $\delta\chi_{\max,i}$.

The parameter $K_{\rm off}$ was adjusted for the small system sizes, through trial runs, so as to minimize the errors in $\chi_{\max}$, while its value for the larger systems was extrapolated from the smaller ones. For $c = p = 0.6$ we set $K_{\rm off} \approx 0.27 l^{-1.66}$, and for $p = 0.8$ $K_{\rm off} \approx 0.12 l^{-1.63}$. The optimal value of $K_{\rm off}$ was found not to depend strongly on the simulation length. The resolution r was adjusted so as to be approximately equal to the ensemble average statistical error of $K^j_{\max}$. Note that the parameters $K_{\rm off}$ and r were set once for each model and each lattice size and were not varied for different samples. In some of the larger systems, for a subset of the samples, the simulation with five times as many Monte Carlo steps was not performed, so that error estimates of $K_{\max}$ and $\chi_{\max}$ were not obtained. This was done in order to save computer time. For these samples the average squared error of $K_{\max}$ and $\chi_{\max}$ was approximated as being six times larger than that of the complementary subset of samples where the error was calculated (from an altogether six times longer Monte Carlo sequence). For the $p = 0.6$ $l = 80$ system the estimated average squared error was extrapolated from the smaller systems.

B. Scaling of $t_c(l)$

In the finite size scaling theory of [9] it was assumed that the average pseudocritical temperature $K_{\max}(l) \equiv [K_{\max}(i,l)]$ scaled as

$$K_{\max}(l) - K_c = A_K l^{-\lambda}, \tag{30}$$

and that the shift exponent [44] $\lambda = y_t = 1/\nu$. First we assumed the correctness of the critical temperature values T_c^∞ quoted in Table II, so that the critical inverse temperature of the infinite sample is assumed to be $K_c = 1/T_c^\infty = 0.285\,781(40)$ for $p = 0.8$, and $K_c = 0.412\,88(10)$ for $c = 0.6$ and $p = 0.6$. Fitting $K_{\max}(l)$ to (30) with K_c fixed we found for the $p = 0.8$ model values of $\lambda = 1.446(34)$ and $A_K = 0.040(5)$ from lattice sizes $16 \leqslant l \leqslant 64$. For the $c = 0.6$ and $p = 0.6$ models the results were incompatible with the fixed value of $K_c = 0.412\,88$. In fact in these models $K_{\max}(l)$ monotonically decreases with l and for the largest lattices we have $K_{\max}(80, p = 0.6) - K_c = -0.000\,26(3)$ and $K_{\max}(60, c = 0.6) - K_c = -0.000\,077(35)$. Thus we also fitted $K_{\max}(l)$ to Eq. (30) with K_c being a free parameter. The values of λ and K_c which were found, using lattice sizes $10 \leqslant l \leqslant 60$ for $c = 0.6$ and $p = 0.6$, and $8 \leqslant l \leqslant 64$ for $p = 0.8$, are given in the third and fourth columns of Table V. For $p = 0.8$ our estimate $K_c = 0.285\,7609(4)$ is within errors of the estimate of Heuer [32] (with canonical disorder) and of Wang *et al.* [35] (with grand canonical disorder). For $c = 0.6$ and $p = 0.6$ our estimates $K_c = 0.412\,54(13)$ and $K_c = 0.412\,51(5)$ are within errors of each other but not within errors of the assumed value $K_c = 0.412\,88(10)$. A more accurate estimate of K_c, which does not require knowledge of λ, is obtained in Sec. V C 1. In the fifth column of Table V estimates of y_t based on estimates of β/ν, ζ/ν and the scaling relation (26) are given. The values of y_t obtained by Heuer in the same way are given in the sixth column of Table V and are compatible with our estimates. Our estimates of y_t and λ agree for $p = 0.8$ (where K_c was fixed) and for $p = 0.6$ (where K_c was a free parameter). For $c = 0.6$ no agreement was found. One possible reason could be that the system size used to estimate λ was too small and that corrections to scaling need to be taken into account. As is well known, finding the critical temperature and the shift exponent simultaneously is a difficult task. In any case, our estimates for y_t are much more accurate than the estimates for λ. It seems to us that trying to extract the shift exponent and the critical temperature by finding the pseudocritical temperature of many samples and using their average $K_{\max}(l)$ in Eq. (30) is not an efficient method. This is because a long MC simulation is needed to avoid systematic errors in esti-

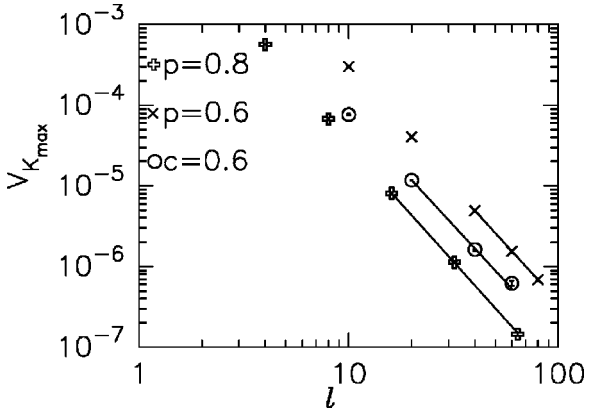

FIG. 8. The variance of the inverse pseudocritical temperatures $V_{K_{\max}}$ as a function of l on a log-log scale. The lines are linear fits yielding exponents ρ_K listed in the last column of Table V.

mating $K_{\max}(i,l)$. Thus it is difficult to obtain a sufficient number of samples for an accurate enough estimate of $K_{\max}(l)$. The error in $K_{\max}(l)$ must be small compared to $K_{\max}(l)-K_c$. This difficulty is not as significant for the estimate of the variance $V_{K_{\max}}$.

C. Variance of pseudocritical temperatures $V_{K_{\max}}$

The variance of the pseudocritical temperatures distribution $V_{K_{\max}}$ was calculated taking into account the errors $[(\delta K_{\max,i})^2]$. This is done in a manner completely analogous to the discussion of V_X in Sec. II C. $V_{K_{\max}}$ is plotted in Fig. 8 on a double logarithmic scale. The solid lines are fits to the form $V_{K_{\max}}=A_K l^{-\rho_K}$ and the resulting estimates of $\rho_K/2$ are listed in the last column of Table V. As one would expect, $V_{K_{\max}}$ is smaller for $c=0.6$ than for $p=0.6$, and is the smallest for $p=0.8$. We see that for all three models the results for ρ_K exclude the possibility (5) that $\rho_K=d=3$. On the other hand $\rho_K/2$ is within errors of y_t for $p=c=0.6$, and within errors of λ (with K_c fixed) for $p=0.8$, as predicted by Aharony and Harris (8). Note that the values obtained for ρ_K for $p=0.8$ with lattices $8\leqslant l\leqslant 32$ and $p=0.6$ with $20\leqslant l\leqslant 60$ are $\rho_K=2.95(6)$ and $\rho_K=3.00(4)$. This behavior of $V_{K_{\max}}$ could be a manifestation of a crossover from pure (5) to dilute (8) critical behavior. On the other hand for the model with the canonical disorder the crossover is in the opposite direction since for $c=0.6$ with $10\leqslant l\leqslant 40$, $\rho_K=2.77(7)$.

The results for $V_{K_{\max}}$ support the picture implied by AH RG calculations, namely, that both the width of the pseudocritical temperatures $\sqrt{V_{K_{\max}}(l)}$ and the distance of its average from the critical inverse coupling $|K_{\max}(l)-K_c|$ scale as $\sim l^{-y_t}$. This is best visualized in Fig. 9 where the frequency of the scaled pseudocritical inverse temperatures $[K_{\max}(i,l)-K_C]l^{y_t}$ is plotted for $p=0.8$ and $l=16,32,64$ with $K_c=0.285\,781$ and $y_t=1.467$. It is evident that the three distributions match well. Their averages are $\{[K_{\max}(i,l)-K_C]l^{y_t}\}=0.047(1),0.0451(28),0.044(5)$, and their widths are $\sqrt{V_{K_{\max}}}l^{y_t}=0.172(15),0.174(28),0.17(4)$ for $l=16,32,64$ respectively. Note that the average ratio of the width to the average is ≈ 3.8. Thus, as is evident from Fig. 9, the fluctuations in $K_c(i,l)$ are significantly larger than

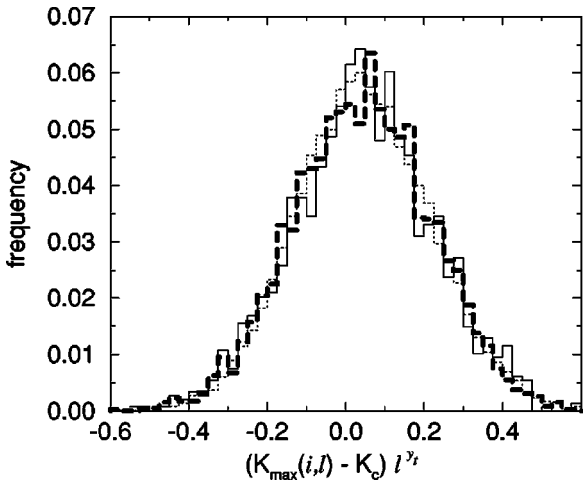

FIG. 9. Frequency distributions of the scaled pseudocritical inverse temperatures $[K_{\max}(i,L)-K_C]^{y_t}$ for $p=0.8$, with $K_c=0.285\,781$ and $y_t=1.467$. Thin dotted line for $l=16$, thick dashed line for $l=32$ and thin solid line for $l=64$. The number of samples used was 32 000 for $l=16$ 4000 for $l=32$ and 1479 for $l=64$.

$|K_c(l)-K_c|$ for any system size. The result is that a measurement of X at the critical temperature T_c^∞ is done in some samples above their pseudocritical temperature $T_c(i,l)$ and in some samples below $T_c(i,l)$.

1. Estimating T_c^∞ through $V_{K_{max}}$

Our estimates of $V_{K_{\max}}$ allow us to estimate T_c^∞ by another method (we thank D. Stauffer for bringing this to our attention). Since asymptotically $K_{\max}(l)-K_c\sim l^{-y_t}$ and $\sqrt{V_{K_{\max}}}\sim l^{-y_t}$, one expects that

$$K_{\max}(l)=K_c+B_v\sqrt{V_{K_{\max}}(l)}, \tag{31}$$

where K_c and B_v need to be determined. Note that by fitting the data according to Eq. (31) (this method was used in percolation studies [45]) it is not necessary to determine ν, and only two fitting parameters are used. Therefore the estimates

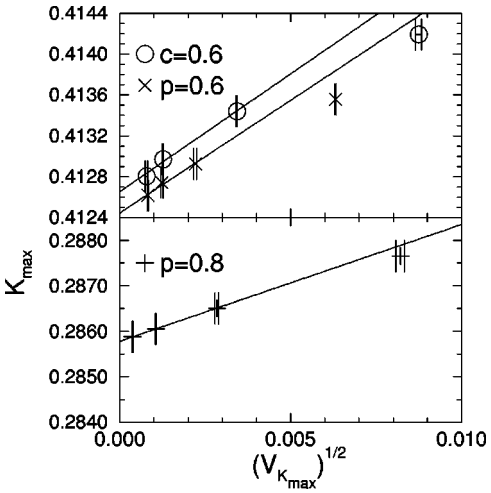

FIG. 10. The average pseudocritical temperature $K_{\max}$ as a function of the square root of $V_{K_{\max}}$ together with linear fits made according to Eq. (31). Fits are made using the three largest system sizes for each model. The fitting parameters are listed in the text.

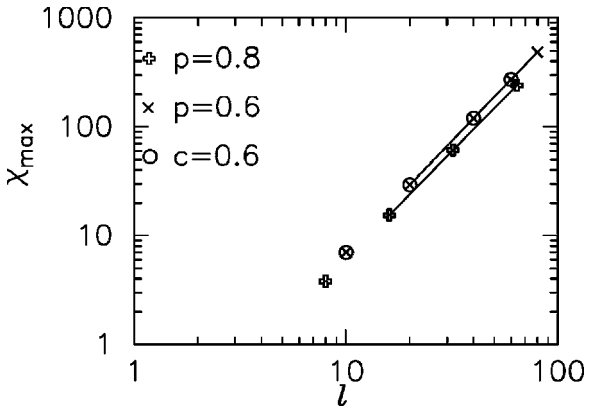

FIG. 11. The ensemble average of the maximum susceptibility $[\chi_{\max}]$ as a function of $\log_{10} l$. The solid lines are fits to the form (16), yielding estimates of $\gamma/\nu = 2.034(2)$ for $c = 0.6$, $\gamma/\nu = 2.027(2)$ for $p = 0.6$, and $\gamma/\nu = 1.987(3)$ for $p = 0.8$.

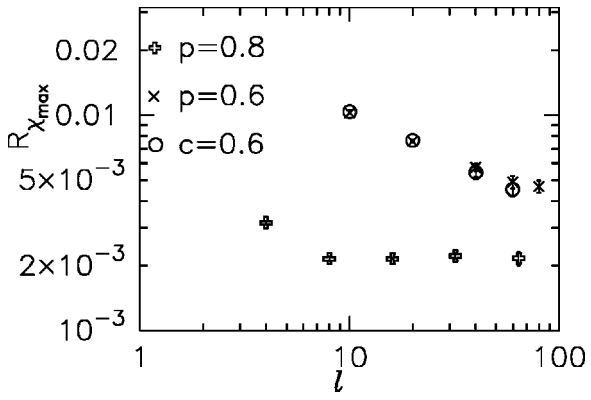

FIG. 12. The relative variance of the maximum susceptibility $R_{\chi_{\max}}$ as a function of $\log_{10} l$.

of K_c obtained in this way are probably more reliable than those given in Table V. In Fig. 10 we plot $K_{\max}$ as a function of $\sqrt{V_{K_{\max}}}$ together with linear fits made according to Eq. (31). We find $K_c = 0.285\,779(2)$, $B_v = 0.257(3)$ for $p = 0.8$, $K_c = 0.412\,44(4)$, $B_v = 0.22(3)$ for $p = 0.6$, and $K_c = 0.412\,65(4)$, $B_v = 0.230(15)$ for $c = 0.6$.

D. Maximum of the susceptibility $\chi_{\max}$

1. Scaling of $[\chi_{max}]$

Another way to study the finite size scaling of the susceptibility is to study the ensemble average of the maximum susceptibility $[\chi_{\max}]$, which is expected to scale with lattice size as in Eq. (16) with a scaling exponent γ/ν. In Fig. 11 $[\chi_{\max}]$ is plotted as a function of l on a double logarithmic scale. The straight lines are linear fits to the form (16). For $p = 0.8$ we find $\gamma/\nu = 1.987(3)$, which is in agreement with the estimate obtained using the susceptibility χ_c at T_c^∞, $\gamma/\nu = 1.990(4)$. As can be seen in Fig. 11 the values of $[\chi_{\max}]$ for $p = 0.6$ and $c = 0.6$ are indistinguishable (they are indeed within errors). This is in contrast with the data at T_c^∞ of Fig. 5 where χ_c of the two models seem to diverge with a similar exponent but with a different amplitude. We have also calculated χ at T_c^∞ and found the same trend, namely, that $\chi(p = 0.6) > \chi(c = 0.6)$, so that this feature is not an artifact of the different definitions, Eqs. (23) and (28), for χ. For $p = 0.6$ and $c = 0.6$ we found $\gamma/\nu = 2.027(2)$ and $\gamma/\nu = 2.034(2)$, respectively. These values are significantly lower than the values found using the susceptibility χ_c at T_c^∞, $\gamma/\nu = 2.104(20)$ and $\gamma/\nu = 2.110(21)$. They are also closer to results of RG calculations $\gamma/\nu = 1.97$ [20,19].

2. Lack of self averaging of the relative variance $R_{\chi_{max}}$

In Fig. 12 we plot the relative variance of the maximal susceptibility $R_{\chi_{\max}}$ as a function of lattice size on a double-logarithmic scale. For $p = 0.8$, $l = 64$ and $p = 0.6$, $l = 80$ we have $[\overline{(\delta\chi_{\max,i})^2}]/V_{\chi_{\max}} \approx \frac{1}{2}, 0.15$, respectively (see Sec. II C). Thus the estimate of $V_{\chi_{\max}}$ is dominated by the estimate of the average squared single sample errors $[\overline{(\delta\chi_{\max,i})^2}]$. For $p = 0.6$ $l = 80$ this estimate was actually extrapolated from the smaller systems estimates (see Sec. V A). Thus these two data points should be taken with more than a grain of salt. It is most interesting to compare Fig. 12 to Fig. 7 where the relative variance of the susceptibility at T_c^∞, R_{χ_c}, is plotted. For $p = 0.8$ the behavior of $R_{\chi_{\max}}$ and R_{χ_c} is qualitatively rather similar. $R_{\chi_{\max}}$ initially decreases as l increases and tends for larger l to a constant, where $R_{\chi_{\max}}(l = 64) = 0.00216(16)$. However, in contrast with Fig. 7, this constant is roughly 72 times smaller than the large l value of R_{χ_c}. This is quite a striking difference. It means that in order to obtain the same relative accuracy in $[\chi_c]$ as in $[\chi_{\max}]$ approximately 70 times as many samples are needed. The source of this difference is apparently simple. The susceptibility of each sample is some function G of the temperature with a sharply peaked maximum at $T_c(i,l)$. In fact G is approximately only a function of the difference $T - T_c(i,l)$, $G\{T - T_c(i,l)\}$. Thus, the value of the maximum susceptibility is nearly sample independent, $\chi_{\max} \approx G(0)$. On the other hand, when one measures χ at T_c^∞, in different samples one is sampling G at different values of its argument. This results in large fluctuations in χ at T_c^∞.

Our findings suggest that the standard procedure of investing much computation time in finding the $l \to \infty$ limit of the critical temperature, T_c^∞, and then averaging quantities at this temperature over many samples, is not optimal. A better procedure may be to locate through the single or multiple histogram method the pseudocritical temperature of each sample, and measure quantities at that temperature. In this way sample to sample fluctuations are reduced substantially and better accuracy is achieved.

For $p = 0.6$ $R_{\chi_{\max}}$ monotonically decreases with lattice size, possibly leveling off to a constant for large l. In contrast with R_{χ_c}, this constant is different from that of the $p = 0.8$ model. Lastly, for $c = 0.6$, in contrast with R_{χ_c}, we find that $R_{\chi_{\max}}$ is within errors of $R_{\chi_{\max}}$ of the $p = 0.6$ model. In addition, $R_{\chi_{\max}}$ initially decreases as l increases, opposite to the behavior of R_{χ_c}. More explanations to the differences in the behavior of $R_{\chi_{\max}}$ and R_{χ_c} are given at the end of the next subsection.

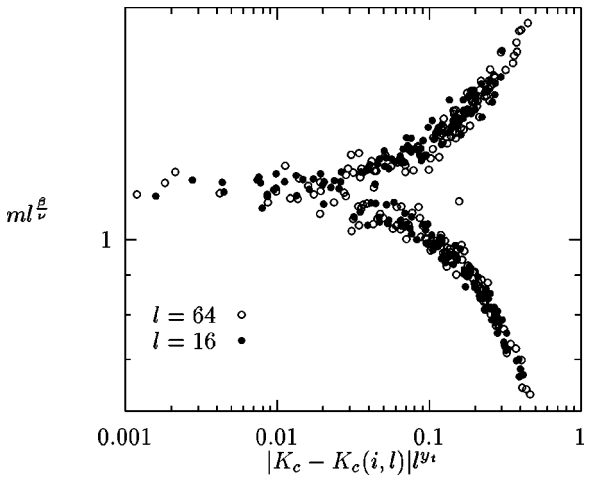

FIG. 13. Scatter plot, where for each sample i the horizontal axis represents the scaled absolute inverse temperature $Z=|K_c-K_c(i,l)|l^{y_t}$ and the vertical axis is the scaled magnetization $\tilde{Q}_{\pm}=ml^{\beta/\nu}$. Points with $K_c>K_c(i,l)$ constitute the higher m (lower temperature) branch, whereas points with $K_c<K_c(i,l)$ constitute the lower m (higher temperature) branch. For the sake of clarity, only 100 points are shown for each system size and each branch, and several points with $|K_c-K_c(i,l)|l^{y_t}<0.001$ were omitted.

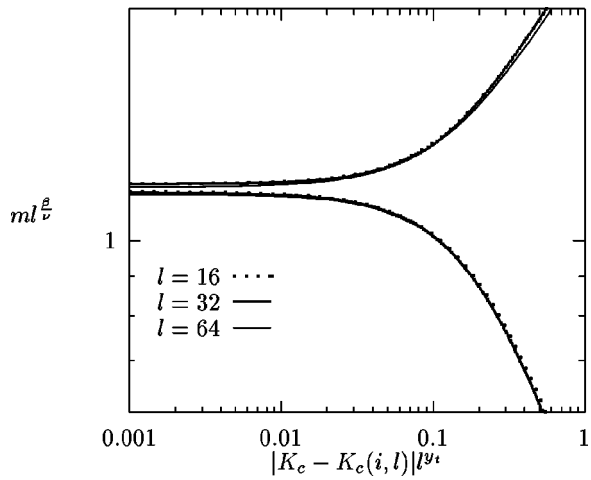

FIG. 14. The functions $\tilde{Q}_{\pm}(Z)$, as defined in (34), obtained from best fits to the scaled magnetization versus temperature scatter plots for $l=16,32,64$. Upper curves according to $\tilde{Q}_{-}$ $[K_c>K_c(i,l)]$ and lower curves according to $\tilde{Q}_{+}$ $[K_c<K_c(i,l)]$. The fitting parameters are given in Table VI.

E. Dependence of $m(T_c^{\infty})$ on $T_c(i,l)$

After examining the behavior of the distribution of $X(i,l)$ at T_c^{∞} and the distribution of $T_c(i,l)$ it is imperative to examine the correlation between the two distributions. A good starting point is the finite size scaling ansatz (4), according to which $X_i(T_c^{\infty})$ mainly depends on $\{T_c^{\infty}-T_c(i,l)\}/T_c^{\infty}$. Figure 13 is a scatter plot where for each sample i the horizontal axis represents the scaled absolute inverse temperature $|K_c-K_c(i,l)|l^{y_t}$ and the vertical axis is the scaled magnetization $m_i l^{\beta/\nu}$. This representation is equivalent to the usual data collapse representation, which is used to demonstrate finite size scaling. The difference is that here the reference critical temperature is $K_c(i,l)$ instead of K_c, and the measurement temperature is always K_c instead of different values of K. Points with $K_c>K_c(i,l)$ constitute the higher m (lower temperature) branch, whereas points with $K_c<K_c(i,l)$ constitute the lower m (higher temperature) branch. In Fig. 13 we plot data for $p=0.8$ and $l=16,64$. For the sake of clarity, only 100 points are shown for each system size and each branch, and several points with $|K_c-K_c(i,l)|l^{y_t}<0.001$ were omitted.

Figure 13 indicates that to a good approximation the scaled magnetization of the sample at T_c^{∞} is a function of only the scaled reduced temperature of the sample. Thus one may attempt to substitute (4) by a sample independent form for $\tilde{Q}_i(Z)$ so that

$$X_i(T,l)\approx l^{\rho}\tilde{Q}(\dot{t}_i l^{y_t}). \tag{32}$$

Note that this is only a good *approximation*; if Eq. (32) were exact, it would mean that $R_{\chi_{\max}}=0$. Thus in order to describe the magnetization data at K_c we write (the change from temperature to inverse temperature is only for convenience)

$$m_i(K,l)=l^{-\beta/\nu}\tilde{Q}_{\pm}(|\{K-K_c(i,l)\}|l^{y_t}). \tag{33}$$

Here $\tilde{Q}_{+}(Z)$ is the scaling function for $K<K_c(i,l)$ and $\tilde{Q}_{-}(Z)$ for $K>K_c(i,l)$. For large l, and thus large Z, the infinite sample critical behavior, $m_i\sim\{K-K_c(i,l)\}^{\beta}$, must be asymptotically reproduced [46] for $K>K_c(i,l)$. Thus, for large Z, $\tilde{Q}_{-}(Z)\sim Z^{\beta}$. For $K<K_c(i,l)$ the shape of $\tilde{Q}_{+}(Z)$ must reproduce, for large Z, the $1/\sqrt{N}$ decay of the magnetization to zero as $l\to\infty$. Thus, for large Z, $\tilde{Q}_{+}(Z)\sim Z^{\beta-d/2y_t}$. For $K=K_c(i,l)$, i.e., $Z=0$, the finite size scaling behavior $[m_i]\sim l^{-\beta/\nu}$ must be asymptotically reproduced, implying $\tilde{Q}_{\pm}(Z)\to$const as $Z\to 0$. (An example of this type of finite size scaling is the scaling we found for $[\chi_{\max}]$.) A simple possible form for $\tilde{Q}_{\pm}(Z)$ fulfilling these requirements is

$$\tilde{Q}_{\pm}(Z)=A_{\pm}Z^{\rho_{\pm}}(1+B_{\pm}Z^{-p_{\pm}})^{\rho_{\pm}/p_{\pm}}, \tag{34}$$

where $\rho_{-}=\beta$ and $\rho_{+}=\beta-d/2y_t$ and $A_{\pm},B_{\pm},p_{\pm}$ are free parameters, so that the data of Fig. 13 should be described by Eqs. (33) and (34) with $K=K_c$. Thus, for each lattice size $l=16,32,64$ and both branches, $K_c<K_c(i,l)$ and $K_c>K_c(i,l)$, the scaled $\{K_{\max}(i,l),m_i(K_c)\}$ pairs (a partial set of which is plotted in Fig. 13) were fitted to the form (34). The values of $\rho_{-}=\beta=0.342\,95$ and $\rho_{+}=\beta-d/2y_t=-0.675\,65$ that were used rely on the finite size scaling results at T_c^{∞} (Tables III and V). The six fitting functions that were obtained are plotted in Fig. 14 and their fitting parameters are given in Table VI. The agreement between the three curves for both branches, as seen in Fig. 14, is surprisingly good. The goodness of the fits is also extremely high. This suggests that Eq. (32), equations similar to Eq. (34), and the possibly invariant (as suggested by Fig. 9) distributions of $K_c(i,l)$ provide an excellent description of the scaling behavior of disordered systems.

TABLE VI. Parameters of the fitting functions $\tilde{Q}_{\pm}(Z)$, defined in Eq. (34), obtained by fitting the data sets of scaled $\{K_{\max}(i,l), m_i(K_c)\}$ pairs for each lattice size $l=16,32,64$ separately (with $p=0.8$). The number of samples used was 32 000, 4000, and 1477 for $l=16$, 32, and 64, respectively. The six fitting functions are plotted in Fig. 14. The crossover lengths, which control the crossover to the large Z behavior, are defined as $Z_{\pm}^{\text{cross}}=B_{\pm}^{1/p_{\pm}}$.

	A_-	B_-	p_-	Z_-^{cross}	A_+	B_+	p_+	Z_+^{cross}
$l=16$	2.387(4)	0.0518(13)	1.45(1)	0.130	0.4695(12)	0.1765(18)	1.299(5)	0.263
$l=32$	2.380(9)	0.048(3)	1.49(3)	0.130	0.4623(22)	0.1687(34)	1.316(9)	0.259
$l=64$	2.291(23)	0.07(1)	1.33(6)	0.142	0.4524(75)	0.152(11)	1.368(35)	0.252

In Fig. 15 we show the same data as in Fig. 13 but for $p=0.6$ and $c=0.6$ with system size $l=40$.

The purpose of this analysis is to demonstrate that the magnetization of the two models is governed by the same temperature dependence, and that the main difference is in the distributions of $K_c(i,l)$. For this reason the data were scaled with the same exponents, taken as the average of the exponents of the two models, $\beta/\nu=0.4375$ and $y_t=1.3905$. In fact our estimates for y_t and β/ν for the two models are within errors. For the sake of clarity, only 100 points for each model and each branch are shown. As was seen with the $p=0.8$ data, it is evident that to a good approximation in both models the magnetization at K_c is a function of only the reduced inverse temperature $K_c-K_c(i,l)$. The main difference between the two models is also clear; for $p=0.6$ there are more points with large $|K_c-K_c(i,l)|$, while for $c=0.6$ there are more points with small $|K_c-K_c(i,l)|$. Thus larger fluctuations for $p=0.6$ in $K_c(i,l)$ (see also Fig. 7) together with the large dependence of $m_i(K_c)$ on $K_c-K_c(i,l)$ give rise to the result that $R_m(p=0.6)>R_m(c=0.6)$.

In Fig. 16 we plot the fitting functions $\tilde{Q}_{\pm}(Z)$, obtained by best fits to the scaled magnetization versus temperature scatter plots for $p=0.6$ and $c=0.6$ with $l=40$ (the full data sets corresponding to Fig. 15).

For the high temperature branch $[K_c<K_c(i,l)$, lower curve] good agreement between the fitting functions $\tilde{Q}_+(Z)$ of the two models is found. For the low temperature branch $[K_c>K_c(i,l)$, higher curve] good agreement is found between the functions $\tilde{Q}_{\pm}(Z)$ for smaller Z, while for large Z $\tilde{Q}_-(Z)$ is larger for the grand canonical disorder ($p=0.6$). The fitting functions $\tilde{Q}_{\pm}(Z)$ for the data for $l=60$ did not agree with those of $l=40$. Possibly this is so because the exponents used are not the asymptotic ones [32,20].

It is also of interest to contrast the dependence of $\chi_{\max}$ on $K_{\max,i}$ with the dependence of $\chi_c(K_c)$ on $K_{\max,i}$. This is a key to understanding the reasons for the differences between the characteristics of R_{χ_c} (Fig. 7) and the characteristics of $R_{\chi_{\max}}$ (Fig. 12). In Fig. 17 we show a scatter plot of $(K_{\max}-K_c, \chi_{\max}/[\chi_{\max}])$ and $(K_{\max}-K_c, \chi_c(K_c)/[\chi_c(K_c)])$ for $p=0.6$ and system size $l=60$ from 950 samples. It is evident that while $\chi_c(K_c)$ shows a strong dependence on $K_{\max}-K_c$, $\chi_{\max}$ shows little dependence on $K_{\max}-K_c$. This qualitative difference persists for all models and all system sizes. This explains why, for any given model, fluctuations in $K_{\max,i}$ give rise to fluctuations in $\chi_c(K_c)$, which are much larger than the fluctuations in $\chi_{\max}$. The result is that $R_{\chi_{\max}} \ll R_{\chi_c}$, as we have noted previously.

Figure 17 is also the key to understanding why $R_{\chi_c}(p=0.6)>R_{\chi_c}(c=0.6)$ while $R_{\chi_{\max}}(p=0.6)\approx R_{\chi_{\max}}(c=0.6)$. In the first case, since fluctuations in $K_{\max}$ are larger for $p=0.6$ than for $c=0.6$ (see Fig. 8) the strong dependence of $\chi_c(K_c)$ on $K_{\max}-K_c$ gives rise to $R_{\chi_c}(p=0.6)>R_{\chi_c}(c$

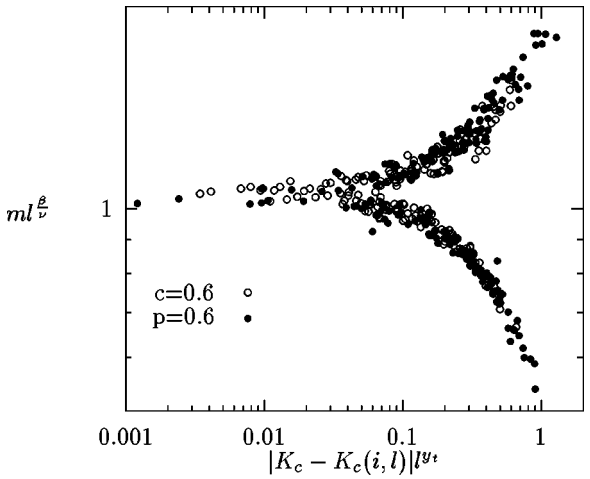

FIG. 15. Same data as in Fig. 13 but for $p=0.6$ and $c=0.6$ with system size $l=40$. The data were scaled with exponents taken as the average of the exponents of the two models, $\beta/\nu=0.4375$ and $y_t=1.3905$. For the sake of clarity, only 100 points for each model and each branch are shown.

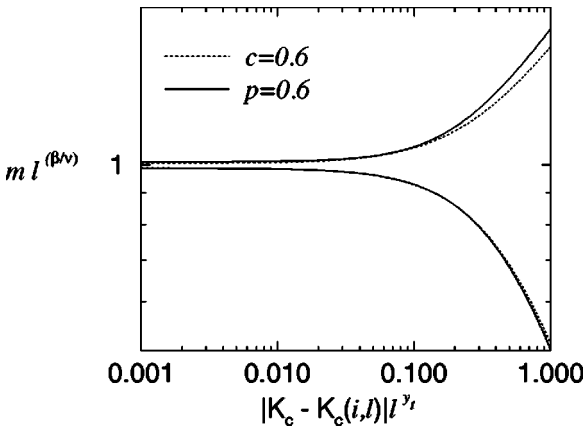

FIG. 16. The functions $\tilde{Q}_{\pm}(Z)$, as defined in Eq. (34), obtained from best fits to the scaled magnetization versus temperature scatter plots for $c=0.6$ (dotted line) and $p=0.6$, with $l=40$. Upper curves according to $\tilde{Q}_-$ $[K_c>K_c(i,l)]$ and lower curves according to $\tilde{Q}_+$ $[K_c<K_c(i,l)]$. Fits made using $\beta/\nu=0.4375$ and $y_t=1.3905$.

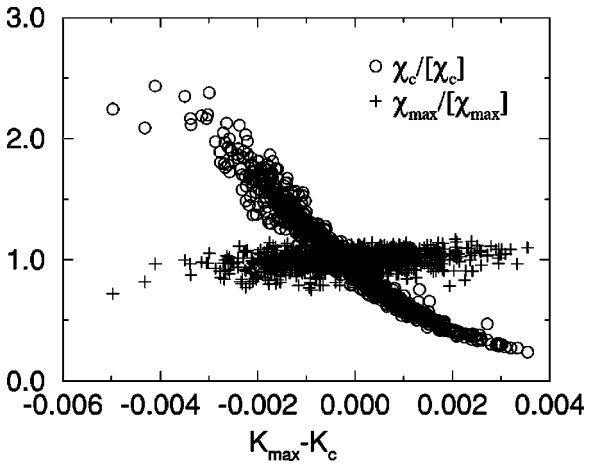

FIG. 17. A scatter plot of $(K_{\max}-K_c, \chi_c(K_c)/[\chi_c(K_c)])$ and $(K_{\max}-K_c, \chi_{\max}/[\chi_{\max}])$, contrasting the dependence of $\chi_c(K_c)$ and $\chi_{\max}$ on $K_{\max}(i,l)$. Data for $p=0.6$ and system size $l=60$ from 950 samples.

$=0.6$). In the second case, despite the fact that fluctuations in $K_{\max}$ are larger for $p=0.6$ than for $c=0.6$, the weak dependence of $\chi_{\max}$ on $K_{\max}-K_c$ results in $R_{\chi_{\max}}(p=0.6) \approx R_{\chi_{\max}}(c=0.6)$.

VI. SUMMARY AND DISCUSSION

By and large it seems that our MC results confirm the AH scenario. In an Ashkin-Teller model, governed by a pure fixed point, we found that $R_X \sim l^{\alpha/\nu}$ in agreement with Eqs. (6) and (7). In site-dilute Ising models on a cubic lattice, governed by a random fixed point, we found a lack of self-averaging for both canonical and grand canonical disorder. One of the aims of our work was to resolve whether at random fixed points our assumption (5), which led to the prediction (6) for the critical width R_X, is correct. The alternative $R_X \to$ const result of AH implies that Eq. (8) should replace Eq. (5). Our results indicate that the AH result is the correct one. Note though that the absolute value of the exponent ratio α/ν of the dilute Ising fixed point, either as calculated by RG, $\alpha/\nu=0.003$, or as indicated by the $p=0.8$ results $\alpha/\nu=-0.055(8)$, is very small. Thus one could argue that our results for R_m and R_{χ_c} do not disprove Eq. (6). The scaling of $V_{K_{\max}}$ is, however, in agreement with Eq. (8) and not with Eq. (5). This therefore rules out Eq. (6) since it is based on Eq. (5).

We find it appropriate to repeat here the results of Aharony and Harris [13], which we have now validated, with an emphasis on the implication to experiments. In finite size scaling form the relative variance can be written as

$$R_X(\xi,l) = l^{\omega} Q(l/\xi). \tag{35}$$

For a fixed $\xi=\xi_0$ and $l \gg \xi$, and thus large Z, strong self-averaging, $R_X(\xi_0,l) \sim l^{-d}$, must be asymptotically reproduced. Thus $Q(Z) \sim Z^{-d-\omega}$ for large Z. At criticality the correlation length diverges and

$$\lim_{\xi \to \infty} R_X(\xi,l) = l^{\omega} Q(0). \tag{36}$$

When the system is governed by a disordered fixed point $\omega=0$. When the system is governed by a pure fixed point $\omega=(\alpha/\nu)_p$. Thus the two possible behaviors for $1 \ll \xi \ll l$ are

$$R_X(\xi,l) \sim \begin{cases} (l/\xi)^{-d} & \text{for a random fixed point} \\ (l/\xi)^{-d} \xi^{\alpha/\nu} & \text{for a pure fixed point .} \end{cases} \tag{37}$$

In an experiment, since generating many samples is impractical, one studies a single large sample with a particular realization of the quenched disorder of size l. For any ξ the value of X measured in the sample is a sampling from a probability distribution with relative variance $R_X(\xi,l)$. Thus $R_X(\xi,l)$ controls the deviation of X from the many samples average. If the system is governed by a random fixed point, as the correlation length is increased, R_X increases as $\sim(l/\xi)^{-d}$. X behaves like the average of $(l/\xi)^d$ independent measurements on regions of size ξ^d. The variance of these measurements does not decrease as ξ increases; it is constant. On the other hand if the disorder is irrelevant and the system is governed by a pure fixed point with $\alpha<0$, as the correlation length is increased, R_X increases more mildly as $\sim(l/\xi)^{-d}\xi^{\alpha/\nu}$. In this case too, X behaves like the average of $(l/\xi)^d$ measurements on regions of size ξ^d. However, as ξ increases, the variance of these measurements decreases as $\sim \xi^{\alpha/\nu}$.

We have verified that for a disordered system governed by a random fixed point $[\delta T_c(l)]^2$ does not scale as $\sim l^{-d}$, but rather as $[\delta T_c(l)]^2 \sim l^{-2/\nu}$. This is an important result, similar to the situation in the purely geometric percolation problem [45]. Recently Pázmándi, Scalettar, and Zimányi [12] claimed that the bound $\nu \geqslant 2/d$, which was supposed to hold for disordered systems [10], is not valid. As they show, if in systems violating this bound one would have $[\delta T_c(l)]^2 \sim l^{-d}$ [our Eq. (5)], then simulations at T_c^{∞} would not be able to capture the true critical exponents [12]. In fact in [12] Eq. (5) is termed ''the most likely scenario'' and the conclusion drawn is that ''self-averaging breaks down.'' However, studies of percolation [45], our results, and those of AH [13] imply the contrary. $[\delta T_c(l)]^2 \sim l^{-2/\nu}$ [our Eq. (8)], and therefore simulations at T_c^{∞} are able to capture the true critical exponents even if $\nu<2/d$. This also becomes evident by examining the finite size scaling theory of [9] for $[X_i(T_c^{\infty})]$, assuming that Eq. (5) holds versus the consequences of Eq. (8).

We have shown that fluctuations in X_i at T_c^{∞} are predominantly due to fluctuations in $\delta T_i = T_c^{\infty} - T_c(i,l)$, and that these fluctuations can be dramatically reduced by measuring X_i at $T_c(i,l)$. This suggests that using the histogram method to obtain $X_i(T_c(i,l))$ for each sample might be a better strategy for Monte Carlo studies than the current strategy of studying $X_i(T_c^{\infty})$. It was also shown that to a good approximation, fluctuations of X_i close to criticality can be accounted for by the finite size scaling form Eq. (32). We believe that a more extensive study of the finite size scaling of sample to sample fluctuations is both feasible and desired.

One of the surprising results of this work is the difference found between the $p=0.6$ model with grand canonical disorder and the $c=0.6$ model with canonical disorder. Our results indicate that for $p=0.6$ and $c=0.6$ $V_{K_{\max}}$ scales as

l^{-2y_t} and that $V_{K_{\max}}(p=0.6)/V_{K_{\max}}(c=0.6)\approx 3.26$. This is apparently the reason why for these two types of disorder R_X tends for large l to different constants. On the other hand we did not find any difference in the scaling exponents of the two types of disorder.

Note added. According to an RG calculation [41], completed after our initial submission, the two models flow under RG to the same grand canonical disorder fixed point. In addition, R_X of the canonical disorder tends to the grand canonical value very slowly, i.e., as $l^{\alpha/\nu}$. This could explain our numerical findings for R_X with $l \leqslant 90$.

ACKNOWLEDGMENTS

We thank A. Aharony, K. Binder, A.B. Harris, W. Janke, M. Picco, and D. Stauffer for useful discussions and suggestions, H.O. Heuer for correspondence, and D. Lellouch for advice on statistics. This research has been supported in part by the Germany-Israel Science Foundation (GIF) and in part by the Israel Ministry of Science. Computations were performed in part on the Paragon at the HLRZ, Jülich, and in part on the SP2 at the Inter-University High Performance Computing Center, Tel Aviv.

[1] R.B. Stinchcombe , in *Phase Transitions and Critical Phenomena*, edited by C. Domb and J.L. Lebowitz (Academic, New York, 1983), Vol. 7.

[2] B.N. Shalaev, Phys. Rep. **237**, 129 (1994).

[3] W. Selke, L.N. Schur, and A.L. Talapov, in *Annual Reviews of Computational Physics*, edited by D. Stauffer (World Scientific, Singapore, 1994), p. 17.

[4] A.B. Harris J. Phys. C **7**, 1671 (1974).

[5] W. Kinzel and E. Domany Phys. Rev. B **23**, 3421 (1981).

[6] K. Binder and A.P. Young, Rev. Mod. Phys. **58**, 837 (1986), and references therein.

[7] R. Brout, Phys. Rev. **115**, 824 (1959).

[8] K. Binder and D.W. Heermann, *Monte Carlo Simulations in Statistical Physics* (Springer-Verlag, Berlin, 1988).

[9] S. Wiseman and E. Domany Phys. Rev. E **52**, 3469 (1995).

[10] J.T. Chayes, L. Chayes, D.S. Fisher, and T. Spencer, Phys. Rev. Lett. **57**, 2999 (1986).

[11] R.R.P. Singh and M.E. Fisher Phys. Rev. Lett. **60**, 548 (1988).

[12] F. Pázmándi, R.T. Scalettar, and G.T. Zimányi, Phys. Rev. Lett. **79**, 5130 (1997).

[13] A. Aharony and A.B. Harris, Phys. Rev. Lett. **77**, 3700 (1996).

[14] Vik S. Dotsenko and Vl S. Dotsenko, J. Phys. A **17**, L301 (1984).

[15] John Cardy (private communication).

[16] S. Wiseman and E. Domany, Phys. Rev. E **51**, 3074 (1995).

[17] O. Dillmann, W. Janke, and K. Binder, J. Stat. Phys. (to be published).

[18] See, e.g., M.E. Fisher, Rev. Mod. Phys. **46**, 597 (1974).

[19] I.O. Mayer, J. Phys. A **22**, 2815 (1989).

[20] H.K. Janssen, K. Oerding, and E. Sengespeick, J. Phys. A **28**, 6073 (1995).

[21] A.M. Ferrenberg and R.H. Swendsen, Phys. Rev. Lett. **61**, 2635 (1988).

[22] A.M. Ferrenberg and D.P. Landau, Phys. Rev. B **44**, 5081 (1991).

[23] E.P. Munger and M.A. Novotny, Phys. Rev. B **43**, 5773 (1991).

[24] R.H. Swendsen, Physica A **194**, 53 (1993).

[25] A.M. Ferrenberg, D.P. Landau, and R.H. Swendsen, Phys. Rev. E **51**, 5092 (1995).

[26] J. Ashkin and E. Teller, Phys. Rev. **64**, 178 (1943).

[27] R.J. Baxter, *Exactly Solved Models in Statistical Mechanics* (Academic, New York, 1982).

[28] B. Nienhuis, in *Phase Transitions and Critical Phenomena*, edited by C. Domb and J.L. Lebowitz (Academic, New York, 1987), Vol. 11.

[29] S. Wang and R.H. Swendsen, Physica A **167**, 565 (1990).

[30] U. Wolff, Phys. Rev. Lett. **62**, 361 (1989).

[31] D.A.S. Fraser, *Statistics an Introduction* (Wiley & Sons, New York, 1958), p. 141.

[32] H.O. Heuer, J. Phys. A **26**, L333 (1993).

[33] J.S. Wang and D. Chowdhury, J. Phys. (France) **50**, 2905 (1989).

[34] T. Holey and M. Fahnle, Phys. Rev. B **41**, 11 709 (1990).

[35] J.S. Wang, M. Wohlert, H. Muhlenbein, and D. Chowdhury, Physica A **166**, 173 (1990).

[36] A. Weyersberg, T. Holey, and M. Fahnle, J. Stat. Phys. **66**, 133 (1992).

[37] M. Hennecke, Phys. Rev. B **48**, 6271 (1993).

[38] M. Hennecke and U. Heyken, J. Stat. Phys. **72**, 829 (1993).

[39] A.M. Ferrenberg, D.P. Landau, and K. Binder, J. Stat. Phys. **63**, 867 (1991).

[40] H.O. Heuer, Phys. Rev. B **42**, 6476 (1990).

[41] A. Aharony, A. B. Harris, and S. Wiseman, Phys. Rev. Lett. **81**, 252 (1998).

[42] A. Aharony (private communication).

[43] S. Chen, A.M. Ferrenberg, and D.P. Landau, Phys. Rev. E **52**, 1377 (1995).

[44] M.N. Barber, in *Phase Transitions and Critical Phenomena*, edited by C. Domb and J.L. Lebowitz (Academic, New York, 1983), Vol. 8.

[45] D. Stauffer and A. Aharony, *Introduction to Percolation Theory* (Taylor & Francis, London, 1992), p. 74.

[46] D.P. Landau, Phys. Rev. B **13**, 2997 (1976).

[47] S. Wiseman and E. Domany, Phys. Rev. Lett. **81**, 22 (1998).